Instability in micromachined curved thermal bimorph structures

2003 J. Micromech. Microeng. 13 955

(http://iopscience.iop.org/0960-1317/13/6/319)

INSTITUTE OF PHYSICS PUBLISHING JOURNAL OF MICROMECHANICS AND MICROENGINEERING

J. Micromech. Microeng. **13** (2003) 955–962 PII: S0960-1317(03)63009-3

Instability in micromachined curved thermal bimorph structures

Chenpeng Hsu and Wensyang Hsu

Department of Mechanical Engineering, National Chiao Tung University, 1001 Ta Hsueh Road, Hsinchu, Taiwan 30010, Republic of China

E-mail: whsu@mail.nctu.edu.tw

Received 2 May 2003
Published 14 August 2003
Online at stacks.iop.org/JMM/13/955

Abstract

For the micromachined thermal bimorph structure, there is often initial deflection, or so-called geometrical imperfection, which may affect the stability of the structure. Here, finite element simulations and experiments are conducted to study the influences of initial deflection and actuating region on mechanical behaviors of a curved bimorph structure with clamped boundary condition. Devices are fabricated by adjusting the internal stresses of polysilicon layers on bimorph structures to achieve various initial deflections. Various actuation regions are achieved by designing different sizes of top layers covering the bottom layers of the bimorph structures. Stable and unstable regions in terms of two design factors, initial deflection ratio and bimorph ratio, are characterized by simulations and experiments. It is found that the curved bimorph structure is stable when the bottom layer is fully covered with the top layer or the initial deflection is much smaller than the structure thickness. The stable device is found to deflect in one direction only. The bimorph structure becomes unstable while the initial deflection is close to or larger than structure thickness. For unstable curved bimorph structures, we find the snap buckling effect with two-way deflections and a hysteresis loop.

(Some figures in this article are in colour only in the electronic version)

1. Introduction

Thermal bimorph effects have been applied widely to micro-actuators for large deflections and moderate forces under IC-level low driving voltages. One typical structure type used in thermal bimorph actuation is the cantilever structure [1–6]. Thermal bimorph structures with beam and membrane types are also found in many applications [7–12].

Analytical solutions to describe the tip deflections and forces of thermal bimorph cantilevers have been discussed [1, 13, 14]. Analyses on flat bimorph beam and circular plate have been developed [13, 15]. Thermal buckling of a curved bimorph beam and a circular plate has been derived for simply-supported boundary conditions under uniform temperature differentials [13, 16–18]. It was pointed out that snap buckling or instability occurs for a simply-supported curved bimorph structure only with the material combination of a large difference in coefficient of thermal expansion (CTE) [18].

However, in micromachined thermal bimorph structures, it is hard to fabricate bimorph structures with simply-supported boundary conditions, because most micromachined bimorph structures have a high slenderness ratio (structural length over radius of gyration of beam cross section), which is closer to clamped boundary conditions [19–21]. Puers *et al* [8] have reported on the effects of thermal expansion against the clamped wall on the behaviors of bimorph structures in different sizes. As they pointed out, thermal expansion becomes important while the size of the bimorph structure decreases. However, there has been no report yet of a study of the instability of micromachined curved bimorph structures with clamped ends.

Here, the mechanical behaviors of curved bimorph structures with clamped ends under different actuating regions are investigated analytically and experimentally. Finite element models are built for simulations. In experiments, curved bimorph structures are micromachined and tested. Two

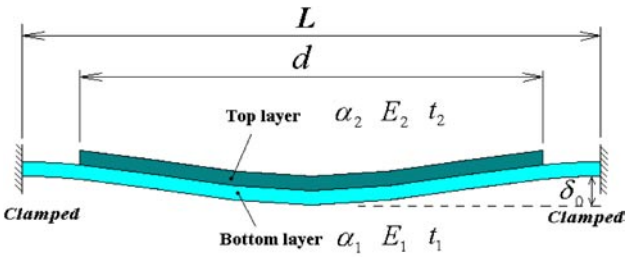

Figure 1. Configurations and structural parameter definitions of the central actuating bimorph structure model.

Table 1. Major material properties used in FEM analysis.

	Polysilicon	Aluminum
Young's modulus E (GPa)	160 (E_1)	69 (E_2)
Density ρ (kg m^{-3})	8910	2700
Poisson's ratio ν	0.26	0.334
CTE α (10^{-6} °C^{-1})	2.33 (α_1)	23.2 (α_2)

crucial factors, the initial deflection ratio and the bimorph ratio, show strong influences on the structural stability of the thermal bimorph structures in both simulations and experiments. The hysteresis effect shown in this investigation due to the combined effects of these two factors would be helpful in explaining the experimental data of previous literature [11].

2. Finite element analysis

2.1. Finite element model

Commercial software ANSYS 5.5 is used to study the mechanical behaviors of curved thermal bimorph structures with clamped ends. The finite element model is built with an eight-node three-dimensional (3D) structural solid element, SOLID45. Nonlinear buckling analysis is performed without considering the intrinsic stress in each layer. Stress stiffening and large deformation effects are also included. Only two major layers, an aluminum layer with larger CTE (α_2) on top and a polysilicon layer with smaller CTE (α_1) at the bottom, compose the bimorph structure model. Other layers, such as heating resistors and the electrical isolation layer, are neglected due to their thinner thickness compared to the major layers, and the meander pattern of the resistor is not considered in the model, which could affect the buckling temperature in simulation results. The bimorph structure model is subjected to a uniform elevated temperature load, denoted as ΔT, which is limited in range of –50 °C to +200 °C with a reference temperature of 20 °C. Table 1 lists the major material properties used in simulations.

Figure 1 shows the schematic diagrams of the bimorph structure model where the structural parameters are also defined. The bimorph structure is in concave shape with clamped ends initially. To investigate the actuating region effect, the top layer partially covers the central portion of the bottom layer, which can provide a central actuating mode in simulation. When the top layer covers the bottom layer over more area, a larger actuating region is obtained. The span of the central actuating bimorph structure (L) is fixed at 1000 μm with a 2.0 μm thick (t_2) aluminum layer and a 2.0 μm thick (t_1) polysilicon layer. The parameters δ_0, h, d and L represent initial deflection, total beam thickness (i.e. $h = t_1 + t_2$), the span of the top layer (also the span of the actuating region) and the span of the bottom layer, respectively. The effective slenderness ratio of the bimorph structure model can be expressed as $\sqrt{3}(L/h)$ and is calculated to be 433. This high slenderness ratio ensures that the bimorph structure model can be set to clamp to the substrate regardless of boundary compliance effects. Two crucial design factors, the initial deflection ratio (δ_0/h), denoted as D_r, and the bimorph ratio (d/L), denoted as B_r, are varied to study the influences on mechanical stability. These dimensionless factors, D_r and B_r, are used to indicate the degree of initial deflection and actuating region, respectively. A positive D_r means the bimorph structure is in concave shape initially. In contrast, a negative D_r means the bimorph structure has a convex shape initially. The B_r factor is in the range of 0.0–1.0 where $B_r = 0.0$ and $B_r = 1.0$ refer to bimorph structures without a top layer and with a top layer fully covering the bottom layer, respectively.

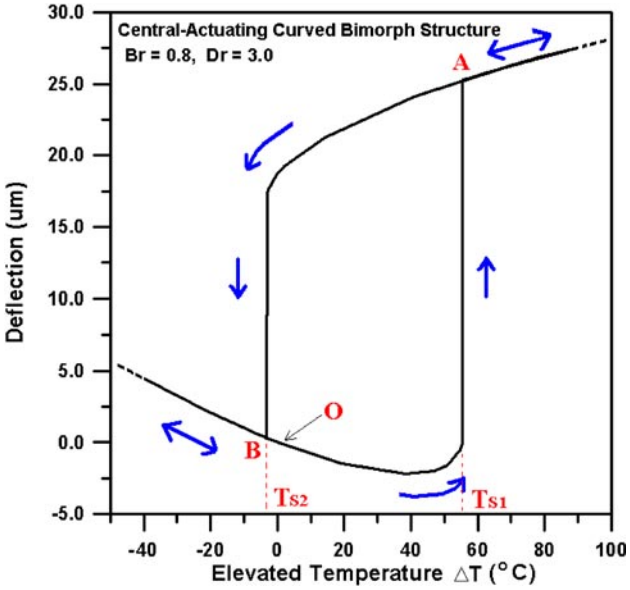

Figure 2. Typical load–deflection curve on the center of a bimorph structure under uniform elevated temperature loads ΔT, where T_{S1} is the forward snap buckling temperature referred to position A and T_{S2} is the snap back temperature referred to position B ($B_r = 0.8$, $D_r = 3.0$).

2.2. Typical load–deflection behaviors

Figure 2 demonstrates simulated typical load–deflection curves on the center of a central actuating bimorph structure subjected to a three-step temperature loading cycle with $D_r = 3.0$ and $B_r = 0.8$. For clarity, only the major part of the load–deflection curves in the temperature range of –40 °C to +90 °C is shown in figure 2. First, the elevated temperature ΔT increases from 0 °C (point O) to 200 °C, then drops from 200 °C to –50 °C, and finally returns to 0 °C. As shown in figure 2, two significant features, two-way deflections and hysteresis loop, are found in snap buckling. It should be pointed out that, when the top layer fully covers the bottom layer ($B_r = 1.0$), the clamped curved bimorph structure would deflect towards the initial deflected direction monotonically.

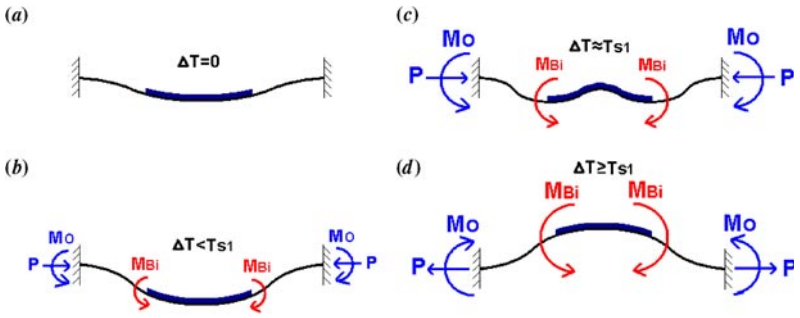

Figure 3. Illustration of the operation principles of the thermal bimorph structure with clamped ends in concave shape initially.

This means that instability will not occur for the clamped and curved bimorph structures with $B_r = 1.0$.

In figure 2, the bimorph structure deflects towards the initial curved direction at first. While ΔT approaches T_{S1}, the bimorph beam stops deflecting in the initial curved direction and starts to deflect in the opposite direction gradually. Once the increasing ΔT reaches and exceeds T_{S1}, the bimorph structure becomes unstable and snaps through to the other side (point A, $\Delta T = T_{S1}$) and then deflects in the post-buckling state with convex shape. In the cooling period, the deflection of the bimorph structure in an upward direction decreases gradually. Similarly, once ΔT is lower than T_{S2}, the bimorph structure becomes unstable and a snap through in a backward direction occurs (point B, $\Delta T = T_{S2}$). When ΔT becomes zero, the bimorph structure returns to its initial position.

In general, the mechanical behaviors can be explained by the equilibrium of three moments, as illustrated in figure 3. The thermal bimorph moment generated on the actuating region of bimorph structure, denoted as M_{Bi}, tends to bend the structure in an opposite or upward direction and causes snap buckling. The reaction moment acting on the ends, denoted as M_O, holds the slope of the clamped ends to be zero. Besides, the reaction force on the ends, denoted as P, would generate bending moment M_P on the whole structure to deflect the curved structure more or to flatten the curved shape depending on the direction of reaction force P. While the elevated temperature ΔT exceeding T_{S1}, moment M_{Bi} overcomes moment M_P and pushes the whole structure to deflect upward suddenly and forward buckling occurs. While the elevated temperature ΔT decreases lower than T_{S2} from a higher temperature, the reducing moment M_{Bi} cannot keep the structure in convex shape any longer and the structure is snapped back by the reaction moment M_O and moment M_P.

2.3. *Effects of initial deflection ratio D_r and bimorph ratio B_r*

The initial deflection ratio D_r is set in the range of 0.1–5.0, and the bimorph ratio B_r is set in the range of 0.2–1.0 in simulations. To study the effects of these two design factors independently, the influences on mechanical behaviors are conducted by fixing one factor and varying values of the other.

Figure 4 shows the simulated load–deflection curves of bimorph structures with $B_r = 0.8$ under various values of D_r. In figure 4, it is shown that a larger D_r factor causes buckling at higher forward snap buckling temperature T_{S1} and lower snap back temperature T_{S2}. This means that the hysteresis loop can be enlarged obviously at a larger D_r factor, i.e. a larger initial

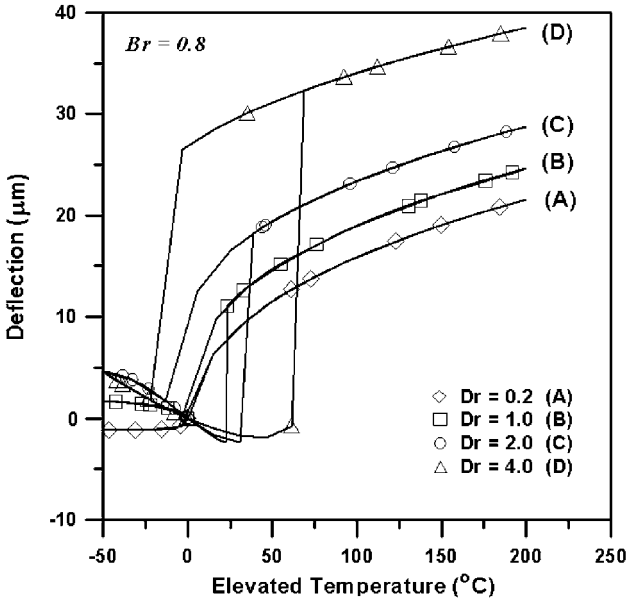

Figure 4. The simulated load–deflection curves of bimorph structures ($B_r = 0.8$) with various values of D_r factor.

deflection. Besides, the deflection stroke, which is defined as the difference on deflections before and after snap buckling, is significantly increased with a larger D_r factor also. When D_r is too small, two-way deflections and snap buckling will not occur, such as in the case with $D_r = 0.2$ in figure 4, where the central actuating bimorph structure deflects upward only; this is similar to the behavior of a central actuating flat bimorph structure [10].

Figure 5 shows the simulated load–deflection curves of bimorph structures with $D_r = 2.0$ under various values of B_r. The forward snap buckling temperature T_{S1} is evidently increased at B_r larger than 0.9. For instance, the temperature T_{S1} is slightly increased from 30.5 to 34.5 °C while B_r is increased from 0.6 to 0.8. However, T_{S1} is significantly increased from 34.5 to 81.7 °C when B_r changes from 0.8 to 0.95. For T_{S2}, the B_r factor does not affect the snap back temperature T_{S2} evidently in general, from 0 to −20 °C as shown in figure 5. But, the deflection stroke will be increased with a larger B_r factor also. As mentioned above, bimorph structures with $B_r = 1.0$ will deflect towards the initial curved direction monotonically and no instability occurs, as shown in figure 5.

Figure 6 summarizes the simulation results, which shows the relations of mechanical stability between the initial

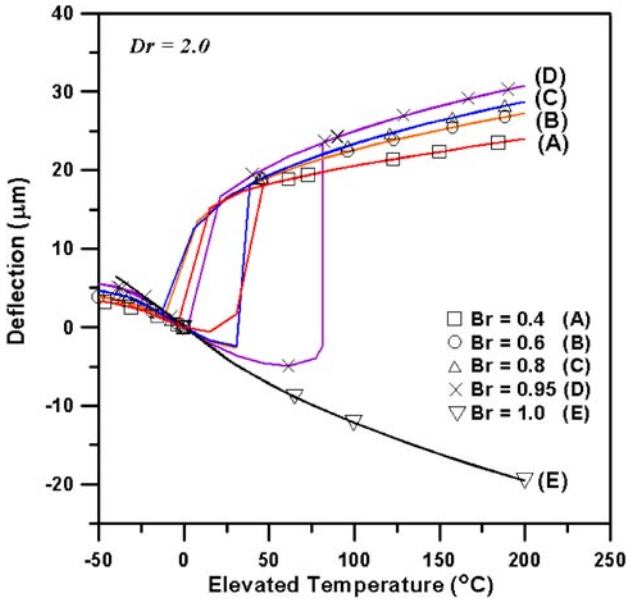

Figure 5. The simulated load–deflection curves of bimorph structures ($D_r = 2.0$) with various values of B_r factor.

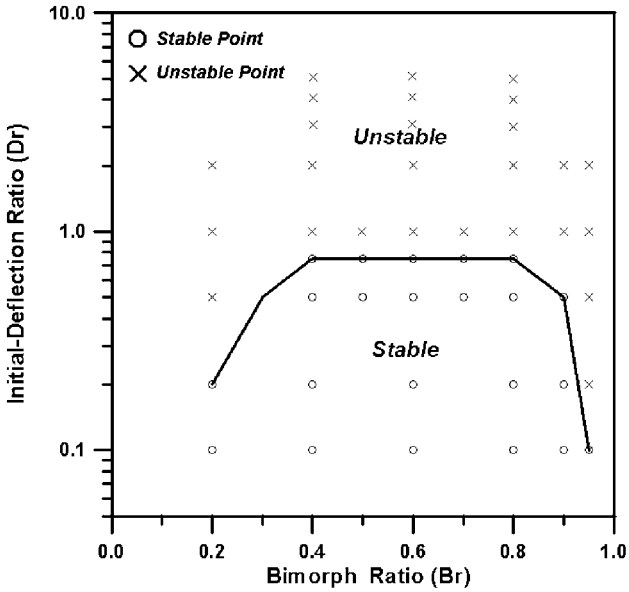

Figure 6. The simulated relations of mechanical stability between the initial deflection ratio D_r and the bimorph ratio B_r. The vertical axis is in log scale.

deflection ratio D_r and the bimorph ratio B_r. The crosses denote unstable cases and the circles represent stable cases. In figure 6, a solid line divides the results into two regions, stable and unstable regions. The plot does not include the cases with B_r equal to 1 and less than 0.2. When there are a combination of design factors located in stable regions, the bimorph structures will deflect in the upward direction only where two-way deflections and snap buckling will not occur. In contrast, for those located in unstable regions, two-way deflections and snap buckling do occur. Furthermore, it should be noted that the bimorph structure becomes unstable while the D_r factor is close to or more than 1. This means that mechanical instability can be induced easily if the initial deflection caused by residual stress in the micromachined bimorph structure is not small enough. Therefore, a bimorph structure with initial deflection much smaller than the structure thickness can avoid unstable behavior. For the actuating region effect, only B_r factors in the range of 0.4–0.8 have wider stable regions. Otherwise, stable regions become very limited for B_r beyond this range.

3. Fabrication considerations and process

We have fabricated central actuating bimorph structures with different initial deflections and actuating regions. The initial deflections are achieved by adjusting internal stresses on structure layers, and the various actuation regions are obtained by designing different sizes of top layers. To fabricate bimorph structures with concave shapes, positive stress gradients must be formed in layered structures. In addition, to achieve different initial deflection ratios, the residual stresses of deposited materials must be adjustable. Hence, low-pressure chemical vapor deposited (LPCVD) polysilicon is chosen as the bottom layer of the bimorph structure owing to its wide range of residual stress [22], which depends on deposition condition and annealing process. Since aluminum has large CTE and is easy to evaporate with high thickness, it is chosen as the top layer of the bimorph structure. Besides, the evaporated aluminum has a tensile residual stress. Therefore, the arrangement of the bottom polysilicon layer in compressive stress and the top aluminum layer in positive stress forms a positive stress gradient that can bend the bimorph structure into the desired concave shape after the stress releasing process.

The curved bimorph structure can be fabricated by surface or bulk micromachining techniques. However, using surface micromachining, the thickness of the sacrificial layer limits the initial downward deflection of the released bimorph structure. Moreover, stiction during and after releasing may occur due to the concave structure shape. Therefore, to simplify the fabrication process, bimorph structures with dimensions of 1×1 mm^2 are fabricated by bulk micromachining with the back-side anisotropic wet etching process.

Figure 7 shows the four-mask fabrication process. First, a 3000 Å thick LPCVD Si_3N_4 layer is deposited on a double-polished 4-inch wafer as an electrical isolation layer and masking layer for back-side anisotropic etching. Then, 2.0 μm thick LPCVD polysilicon is deposited at 620 °C to form a bottom structural layer with highly compressive residual stress. In order to have different initial deflections, the polysilicon layer is then treated by three different heat treatments: without annealing, annealing at 900 °C for 90 min and annealing at 1100 °C for 90 min. Then, the metal heating resistors made of Ti/Au/Ti (250 Å/1500 Å/250 Å) are evaporated and lifted off. Then, 3000 Å thick plasma-enhanced chemical vapor deposited (PECVD) TEOS SiO_2 is deposited and patterned to electrically isolate the metal resistors. Next, 2.0 μm thick aluminum is deposited and patterned as top structural layer. The Si_3N_4 layer on the back side of the wafer is then patterned by reactive ion etching (RIE) to form the etching windows for back-side etching. The anisotropic wet etching is performed in a 25% alkaline solution at 70 °C where a Teflon chuck is used to protect the front-side patterns of the wafer. The Si_3N_4 layer beneath the polysilicon bottom structural layer is then

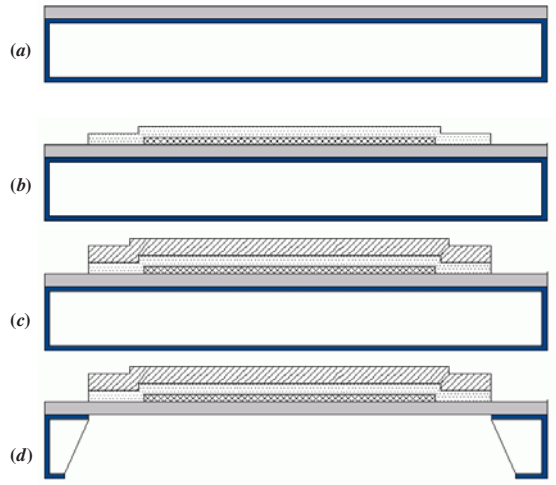

Figure 7. Fabrication process. (*a*) Deposition of LPCVD Si_3N_4 and polysilicon. The polysilicon layer is annealed in furnace, (*b*) evaporation of metal resistors then patterned by lift-off process, (*c*) deposition of PECVD TEOS SiO_2 as electrical isolation layer and patterning and (*d*) backside anisotropic etching with Teflon chuck to protect front-side patterns. The bimorph structures are formed in concave shapes by final Si_3N_4 stripping with RIE.

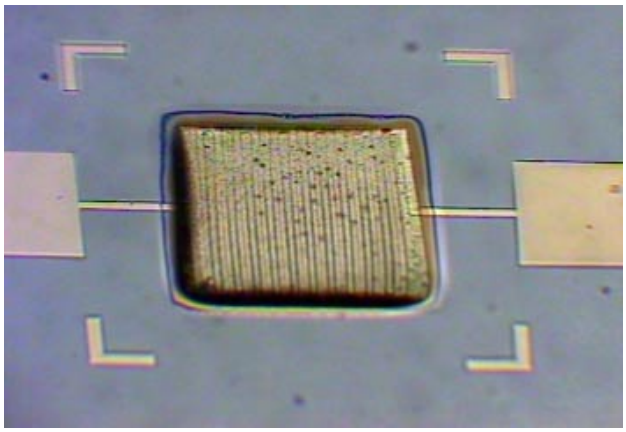

Figure 8. The perspective view of the fabricated curved bimorph structure with a 2.0 μm thick aluminum layer on top and a 2.0 μm thick LPCVD polysilicon layer at bottom ($B_r = 0.8$, $D_r = 3.3$).

stripped using RIE. Finally, bimorph structures with concave shapes are obtained.

4. Testing results and discussion

4.1. Polysilicon/aluminum bimorph structures

Bimorph structures with values of B_r factor in the range of 0.4–1.0 and various initial deflection ratios are fabricated and tested to compare with the simulation results. Figure 8 shows optical photo of a 1 × 1 mm^2 central actuating bimorph structure where the initial curved shape can be observed. In experiments, there are two types of meandering resistor pattern, parallel and spiral, designed to uniformly heat the bimorph structure. The device shown in figure 8 has the meandering resist pattern in parallel. In testing, the two resistor patterns showed no difference in mechanical behaviors of the fabricated devices. The initial deflection ratios of the

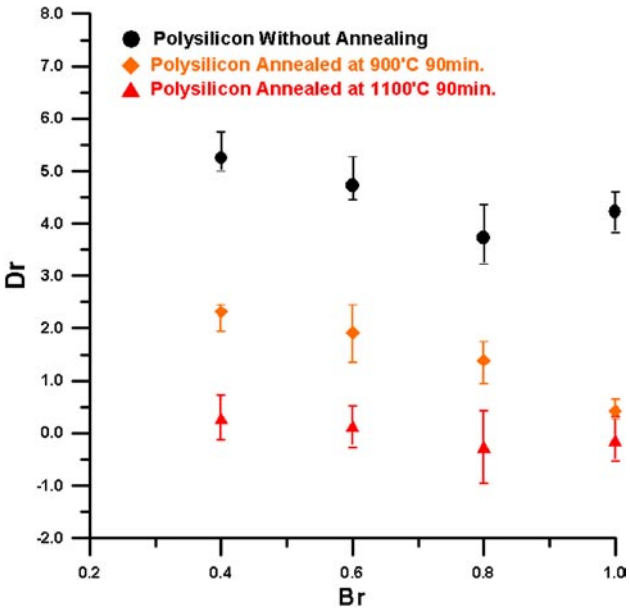

Figure 9. Measured initial deflection ratios of the fabricated bimorph structures with various design factors B_r under different polysilicon annealing temperatures.

fabricated devices are calibrated by optical microscopy with a resolution of ±1.0 μm, as shown in figure 9. The maximum D_r factor up to 5.8 is achieved by the proposed stress adjusting fabrication process. The averaged residual stresses of 2.0 μm thick polysilicon layers measured by the conventional wafer curvature method are −300, −200 and +9 MPa for three different heat treatments, respectively. As mentioned above, the positive value of the D_r factor means that the fabricated device is in the desired concave shape initially. A few devices are observed having convex shape initially with negative D_r factors, which all occurred for devices with polysilicon annealed at 1100 °C for 90 min. From figure 9, it is found that the D_r factor is not only influenced by the polysilicon annealing temperature, but it is also affected by the B_r factor. Under the same heat treatment, the fabricated device with a larger B_r factor leads to a smaller D_r, which results from the higher flexural rigidity of the device due to the large actuating region. In general, a higher annealing temperature results in smaller initial deflection.

Static deflections of the fabricated devices with various D_r and B_r factors are measured by a laser confocal displacement meter with a resolution of ±0.2 μm. The effects of the D_r factor have been tested, and are shown in figure 10. The tested results of $B_r = 0.6$ and $B_r = 0.8$ are shown in figures 10(*a*) and (*b*), respectively. The cross near the end point of each curve means that the tested devices are ruptured in buckling due to the large shear stresses generated on the interface between the top and bottom structural layers. Although rupture occurs, the phenomena of two-way deflections and snap buckling are still observed with design factors located in the unstable region predicted in the simulations of figure 6. In figures 10(*a*) and (*b*), the devices with the smallest D_r factors deflect only in the upward direction, which also agrees with the simulation. In experiments, larger electrical powers are required to cause buckling for devices with larger D_r factors, which is also

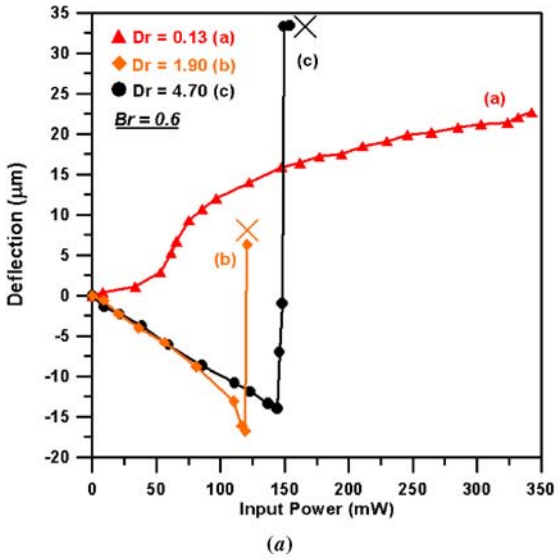

(*a*)

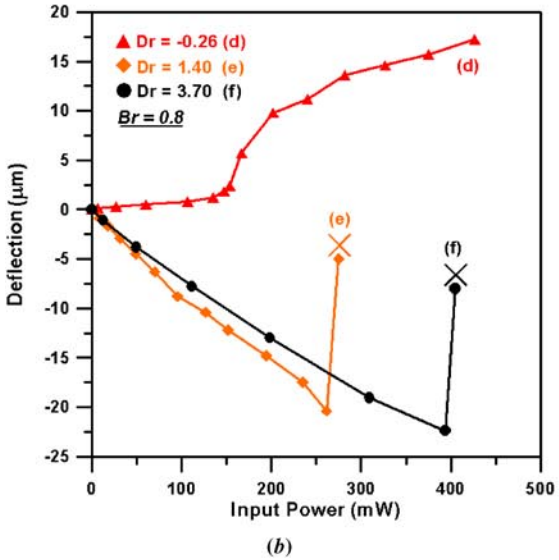

(*b*)

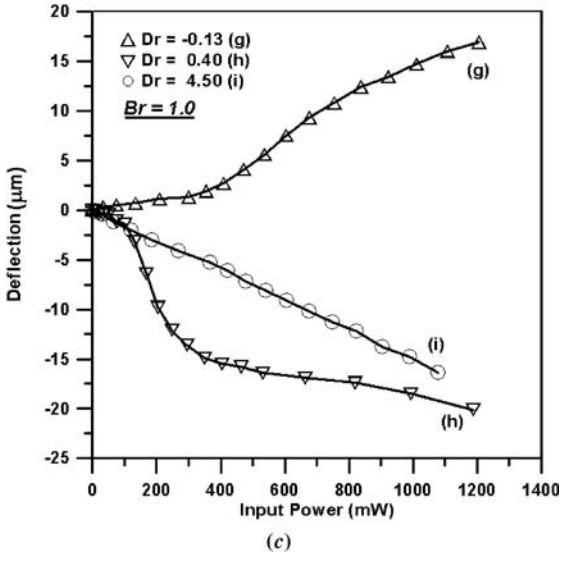

(*c*)

Figure 10. Tested load–deflection curves of bimorph structures at (*a*) $B_r = 0.6$, (*b*) $B_r = 0.8$ and (*c*) $B_r = 1.0$ with different values of D_r factor.

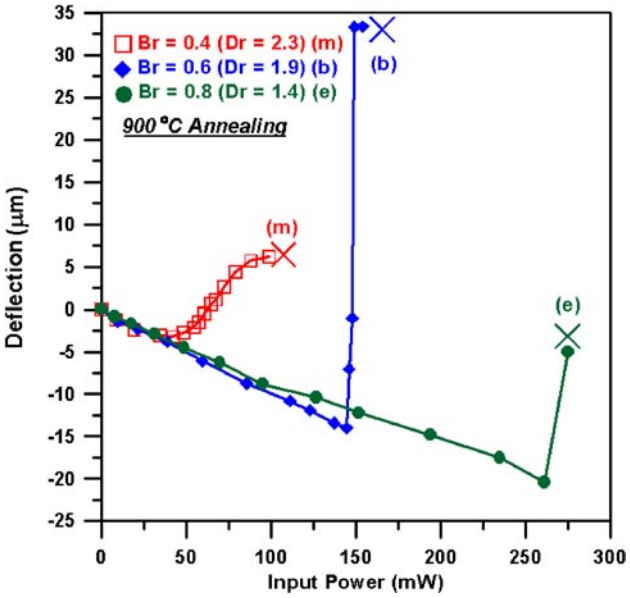

Figure 11. Experimental results on the effects of the bimorph ratio B_r.

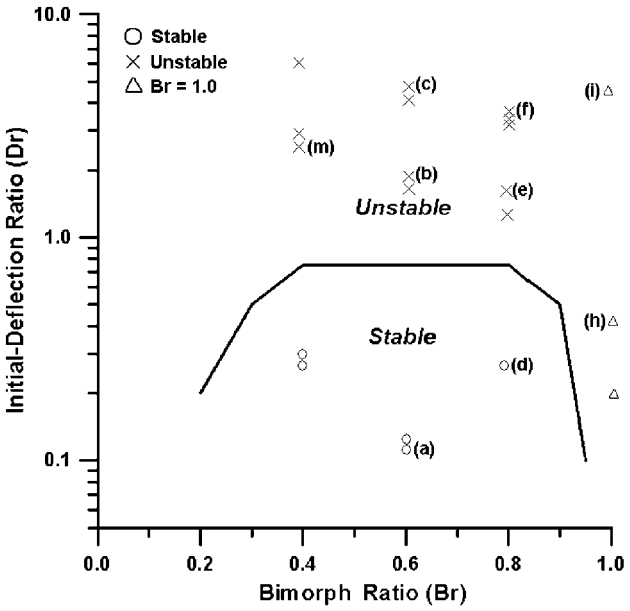

Figure 12. The testing results are shown by different symbols in terms of the initial deflection ratio and bimorph ratio, where the devices in figures 10 and 11 are labeled. The solid line is the simulated results of figure 6, and it divides the plot into two regions.

indicated by simulation results that larger D_r factors lead to higher forward snap buckling temperature T_{S1}.

For a device with $B_r = 1.0$, this means the bottom layer is fully covered by the top layer, and mechanical instability does not occur, as shown in figure 10(*c*). In figure 10(*c*), devices with initial concave and convex shapes are found to deflect only in the downward and upward directions, respectively, despite the D_r values, which all support our simulated mechanical behaviors. The stable device deflects only in the initial curved direction even when the aluminum top layer melts at an applied power over 1200 mW.

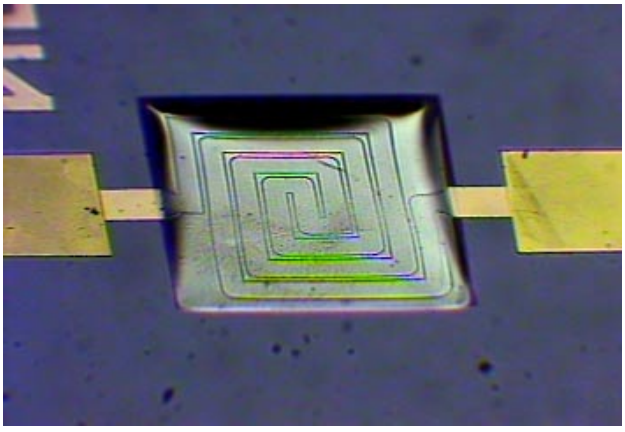

(*a*)

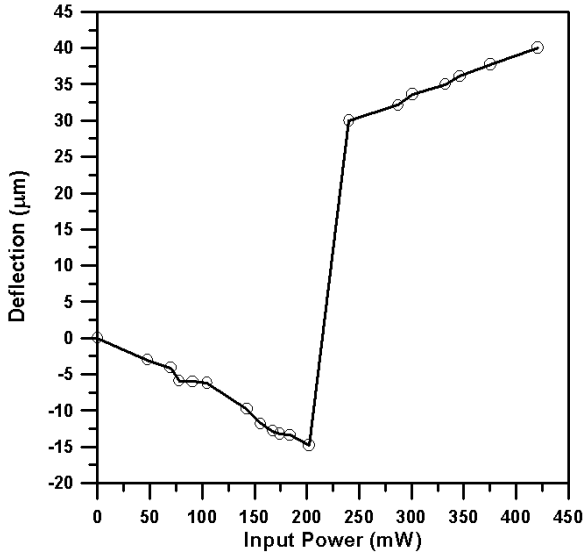

(*b*)

Figure 13. (*a*) A photograph of the fabricated silicon-oxide/aluminum bimorph structure ($B_r = 0.9$, $D_r = 1.8$). (*b*) Measured load–deflection curve of the fabricated device subjected to a loading cycle.

The testing results on the effects of the B_r factor are shown in figure 11. In figure 11, it is shown that snap buckling will occur at higher electrical power for devices with larger B_r, which means a higher snap buckling temperature. Besides, the deflection stroke is enlarged with increasing B_r. Figure 12 summarizes the testing results on stability in terms of the initial deflection ratio D_r and bimorph ratio B_r. As shown in figure 12, the circles, crosses and triangles represent stable, unstable and $B_r = 1.0$, respectively. The measured data shown in figures 10 and 11 are labeled with small letters in figure 12. The solid line, which is the simulation results of figure 6, divides the testing results into stable and unstable regions.

4.2. Silicon-oxide/aluminum bimorph structures

Another bimorph structure made of a 3.1 μm thick silicon-oxide bottom layer and a 1.8 μm thick aluminum top layer has been fabricated and tested. The bottom silicon-oxide layer consists of a thermal-SiO_2/Si_3N_4/PECVD-SiO_2 (1.4 μm/0.3 μm/1.4 μm) layered structure. The residual stress in each layer is hard to modify by heat treatments, therefore only limited D_r values in the range of 1.2–1.8 are available in the fabricated devices. Figure 13(*a*) shows a photograph of the fabricated device, and the testing results are shown in figure 13(*b*). In figure 13(*b*), the two-way deflections, snap buckling and post-buckling behavior are all observed. However, all fabricated devices snap back at driving powers almost the same as in forward snap buckling. Therefore, the hysteresis loop is not obvious because the D_r factor is not large enough. Figure 14 shows different deformation states of the silicon-oxide/aluminum bimorph structure before and after snap buckling. The dark regions in the photographs are due to the scattering of the projected lights on the inclined or deformed structure surfaces.

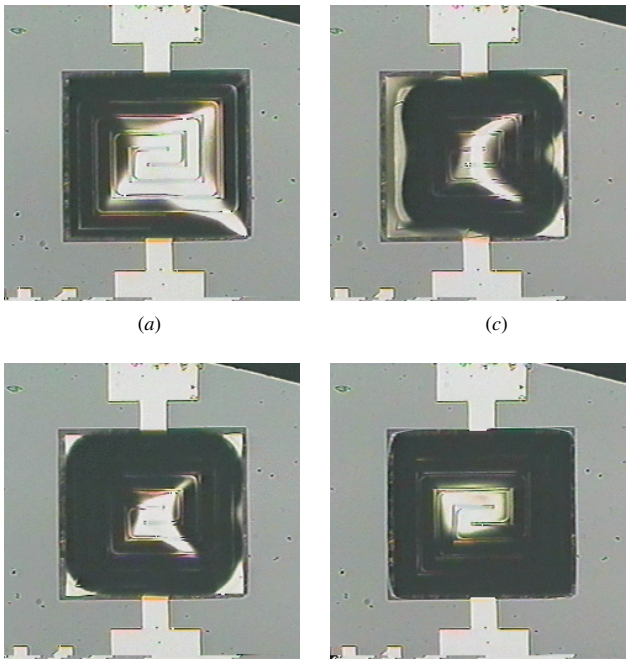

(*a*) (*c*) (*b*) (*d*)

Figure 14. Operation of the initial curved bimorph structure made of silicon-oxide and aluminum: (*a*) before activation (initial concave shape); (*b*) deflecting in downward direction ($T < T_{S1}$); (*c*) asymmetry deformation on just snap buckling ($T \rightarrow T_{S1}$); (*d*) after snap buckling in a convex shape ($T > T_{S1}$).

5. Conclusion

Simulations and experiments are conducted to study the stabilities of micromachined curved thermal bimorph structures with different actuating regions. Two design factors, initial deflection ratio D_r and bimorph ratio B_r, are found to play important roles in the mechanical stability of the clamped bimorph structure. For the bottom layer fully covered by the top layer ($B_r = 1.0$), the bimorph structures are always stable and deflect in the initial curved directions only. For bimorph structures with $B_r < 1.0$, instability may occur when the initial deflection is close to or more than the structure thickness. Unstable behaviors with snap buckling, two-way deflections and hysteresis loop can be found. With a larger D_r factor, structural instability with large stroke is observed

and confirmed. Besides, design factors D_r and B_r are found to have strong influences on hysteresis loops. In general, the loops can be enlarged significantly by increasing values of D_r and B_r factors. The simulation and experimental results discussed in this paper are helpful in designing thermal bimorph micro-actuators and other microelectromechanical systems (MEMS) suspended multilayered structures that may undergo temperature variations.

Acknowledgments

This research was supported in part by the National Science Council of the Republic of China under grant number NSC89-2218-E009-111. The authors would like to thank the staff at the NCTU Nano Facility Center for providing technical support.

References

[1] Riethmüller W and Benecke W 1988 Thermally excited silicon microactuators *IEEE Trans. Electron Devices* **35** 758–62
[2] Buser R A, Rooij N F, Tischhauser H, Dommann A and Staufert G 1992 Biaxial scanning mirror activated by bimorph structures for medical applications *Sensors Actuators* A **31** 29–34
[3] Greitmann G and Buser R A 1995 Tactile microgripper for automated handling of microparts *Transducers'95* pp 372–5
[4] Suh J W, Darling R B, Böhringer K-F, Donald B R, Baltes H and Kovacs G T A 1999 CMOS integrated ciliary actuator array as a general-purpose micromanipulation tool for small objects *J. Microelectromech. Syst.* **8** 483–96
[5] Schweizer S, Cousseau P, Lammel G, Calmes S and Renaud Ph 2000 Two-dimensional thermally actuated optical microprojector *Sensors Actuators* A **85** 424–9
[6] Huja M and Husak M 2001 Thermal microactuators for optical purpose *Proc. Micro Electromechanical Systems'01* pp 137–42
[7] Jerman H 1994 Electrically-activated normally-closed diaphragm valves *J. Micromech. Microeng.* **4** 210–6
[8] Puers R, Cozma A and Bruyker D D 1998 On the mechanisms in the thermally actuated composite diaphragms *Sensors Actuators* A **67** 13–7
[9] Zou Q, Sridhar U and Lin R 1999 A study on micromachined bimetallic actuation *Sensors Actuators* A **78** 212–9
[10] Hsu C and Hsu W 2000 A two-way membrane-type micro-actuator with continuous deflections *J. Micromech. Microeng.* **10** 387–94
[11] Sehr H, Evans A G R, Brunnschweiler A, Ensell G J and Niblock T E G 2001 Fabrication test of thermal vertical bimorph actuators for movement in the wafer plane *J. Micromech. Microeng.* **11** 306–10
[12] Izumida K, Toyota N, Yoshimura M and Muroi Y 2001 Micro generator systems *Transducers'01* pp 42–5
[13] Timoshenko S P 1925 Analysis of bi-metal thermostats *J. Opt. Soc. Am.* **11** 233–5
[14] Chu W-H, Mehregany M and Mullen R L 1993 Analysis of tip deflection orce of a bimetallic cantilever microactuator *J. Micromech. Microeng.* **3** 4–7
[15] Young W C 1989 *Roark's Formulas for Stress & Strain* (New York: McGraw-Hill) pp 425–51
[16] Wittrick W H, Myers D M and Blunden W R 1953 Stability of a bimetallic disk *Q. J. Mech. Appl. Math.* **6** 15–31
[17] Burgreen D and Manitt P J 1969 Thermal buckling of a bimetallic beam *ASCEJ Engineering Mechanics Division* **95** 421–32
[18] Burgreen D and Regal D 1971 Higher mode buckling of bimetallic beam *ASCEJ Engineering Mechanics Division* **97** 1045–56
[19] Gerlach G, Schroth A and Pertsch P 1996 Influence of clamping conditions on microstructure compliance *Sensors Mater.* **8** 79–98
[20] Kobrinsky M, Deutsch E R and Senturia S D 2000 Effect of support compliance residual stress on the shape of doubly supported surface-micromachined beams *J. Microelectromech. Syst.* **9** 361–9
[21] Beer F P and Johnston E R 1992 *Mechanics of Materials* 2nd edn (New York: McGraw-Hill)
[22] Madou M 1997 *Fundamentals of Microfabrication* 1st edn (Boca Raton, FL: CRC Press)